

Lithos

October 2018, Volume 318-319 Pages 219-229

<http://dx.doi.org/10.1016/j.lithos.2018.08.021><http://archimer.ifremer.fr/doc/00457/56903/>

© 2018 Elsevier B.V. All rights reserved.

Archimer<http://archimer.ifremer.fr>

Ediacaran to lower Cambrian basement in eastern George V Land (Antarctica): Evidence from U Pb dating of gneiss xenoliths and implications for the South Australia- East Antarctica connection

Lamarque Gaëlle ^{1,2,*}, Bascou Jérôme ¹, Ménot René-Pierre ¹, Paquette Jean-Louis ³,
Couzinié Simon ⁴, Rolland Yann ⁵, Cottin Jean-Yves ¹

¹ Université de Lyon, UJM Saint-Etienne, UMR CNRS IRD 6524, Laboratoire Magmas et Volcans, F-42023 Saint-Etienne, France

² Ifremer, Geosciences Marines, Centre de Brest, 29280 Plouzané, France

³ UMR CNRS IRD 6524, Laboratoire Magmas et Volcans, 63038 Clermont-Ferrand, France

⁴ Université de Lyon, ENSL, UCBL, CNRS, LGL-TPE, 69007 Lyon, France

⁵ Université de Nice-Sophia Antipolis, Géoazur, UMR CNRS 7329, 250 rue Albert Einstein, 06560 Valbonne, France

* Corresponding author : Gaëlle Lamarque, email address : gaelle.lamarque@ifremer.fr

Abstract :

This study presents the first geochronological results on basement rocks from the Penguin-Bage-Webb (PBW) domain located east of the Neoproterozoic Terre Adélie craton, Antarctica. Investigated samples are paragneiss xenoliths hosted within early Paleozoic granitoids, which were emplaced during the Ross orogeny. Zircon UPb dating yielded ages ranging from the Archean to the Cambrian, with a dominant Ediacaran (550–635 Ma) population and maximum depositional ages around 570–575 Ma. U–Th–Pb analyses of monazite suggest that the metamorphic event that formed the gneiss samples occurred at ca. 515 Ma, shortly prior to incorporation within the granitic magmas. The studied samples likely represent relics of the pre-Gondwana Pacific margin, which was subsequently deformed and metamorphosed during the early Paleozoic Ross orogeny. The obtained zircon UPb date distributions present similarities with those of the Kanmantoo and Nargoon sediments in Southern Australia and provide new constraints for the correlations between East Antarctica and South Australia before the opening of the Southern Ocean.

Highlights

► Zircon and monazite U—Pb ages of the gneiss xenoliths from eastern George V Land ► Inherited ages ranging from Archean to Cambrian with main Ediacaran population ► Relics of a pre-Gondwana Pacific margin metamorphosed during the Ross orogeny

Keywords : Gondwana margin, Ross orogeny, George V Land, Antarctica-Australia connection, Zircon and monazite UPb dating

33 **1/ Introduction**

34 The initial configuration of Gondwana and its fragmentation are still debated because of the
35 lack of consensus on the nature of major structures and geological domains that composed the
36 super-continent. In East Gondwana, the region of Terre Adélie and George V Land (East
37 Antarctica) is considered to represent southern extension of South Australia (Borg and
38 DePaolo, 1994; Di Vincenzo et al., 2014; Flöttmann et al., 1993; Oliver and Fanning, 1997;
39 Payne et al., 2009; Peucat et al., 2002, 1999; Reading, 2004; Talarico and Kleinschmidt,

40 2003a), Figure 1. In particular, the continuity of the Terre Adélie Craton in Antarctica with
41 the western Gawler Craton (Australia), both being parts of the Neoproterozoic
42 Mawson Continent, is well documented from geological (Fanning et al., 1999, 2003;
43 Fitzsimons, 2003) and geophysical studies (Aitken et al., 2014). However, the continuity of
44 the domains located east of the Mawson Continent needs to be refined because lacks and
45 inconsistencies exist. For example, outcrops from the eastern Gawler Craton (Australia)
46 characterized by 1.85 and 2.0 Ga ages (Hand et al., 2007), as well as Ediacaran-early
47 Cambrian formations such as Kanmantoo group (Ireland et al., 1998) do not display
48 correlatives neither in eastern George V Land (Antarctica) nor in the Terre Adélie Craton.
49 Furthermore, the lack of geochronological data from eastern George V Land, more
50 specifically on the Penguin-Bage-Webb block (close to the Terre Adélie Craton), is a key
51 issue to better understand the Precambrian connections between Australia and Antarctica and
52 subsequently the evolution of both the Mawson Continent and the Gondwana.
53 The aim of this contribution is thus to constrain the age of the Penguin-Bage-Webb basement
54 block located east of the Terre Adélie Craton and separated from it by the Mertz Shear Zone
55 (Di Vincenzo et al., 2007; Ménot et al., 2007). Up to now, only the cross-cutting granitoids of
56 Penguin Point have been dated by zircon U-Pb analyses at 505 Ma (Fanning et al., 2002) and
57 $508\text{-}510 \pm 5$ Ma (Goodge and Fanning, 2010), and by biotite $\text{Ar}^{39}/\text{Ar}^{40}$ analyses at 487.7 ± 3.5
58 Ma (Di Vincenzo et al., 2007). The existence of gneiss xenoliths within the early Paleozoic
59 granites offers a unique opportunity to clarify the age and nature of the underlying basement
60 which have, up to now, never been addressed. In this study, we report the results of zircon and
61 monazite U-Pb analyses performed on three gneiss xenoliths. The obtained dataset allows to
62 discuss: (i) the potential extension of the Terre Adélie Craton eastward and the role of the
63 Mertz Shear Zone to the tectonic evolution of the area, and, (ii) the correlation between the
64 Penguin-Bage-Webb block and its presumably corresponding Australian formations.

65 **2/ Geological setting**

66 **2.1/ Terre Adélie and George V Land**

67 The Terre Adélie and the western George V Land constitute the Terre Adélie Craton (135 to
68 145°E), which is part of the Neoproterozoic-Paleoproterozoic Mawson continent (Fanning et al.,
69 2003). The Terre Adélie Craton is divided into two domains: the Neoproterozoic basement and
70 the Paleoproterozoic metasedimentary basins (Ménot et al., 2007, see Figures 1, 2). The
71 Neoproterozoic basement (in green and brown on Figure 2) extends from 141°E (the Zélée shear
72 zone, ZSZ) to 146°E (the MSZ) and is predominantly composed of felsic to mafic orthogneiss
73 and granodiorites intruding siliciclastic metasediments with subordinate marbles and calc-
74 silicates. This 2.55-2.44 Ga continental crust segment (Duclaux et al., 2008; Oliver and
75 Fanning, 2002) exposes two distinct tectonic units that equilibrated under granulite and
76 amphibolite facies conditions respectively, and then represent deep and intermediate crustal
77 sections, respectively (Ménot et al., 2005). A thermal and tectonic event occurred at 1.7-1.5
78 Ga, as proposed by Di Vincenzo et al. (2007) on the base of Ar/Ar dating. According to
79 Duclaux et al. (2008), the 1.7 Ga event is likely to be restricted to narrow fluid-bearing
80 anastomosed shear zones, concentrated on the edges of the Neoproterozoic domain (Mertz and
81 Zélée shear zones). Synchronously to this event, the Paleoproterozoic metasedimentary basins
82 were formed (purple in Figure 2). They include the Dumont d'Urville (DDU) and Cape
83 Hunter (CH) basins. DDU basin extends west from 141°E (the Zélée shear zone) and consists
84 of dominant metapelitic migmatitic gneisses together with minor metagraywackes, silicic
85 metavolcanics and mafic intrusions. The DDU formations experienced high-grade
86 amphibolite-facies metamorphic conditions (Pelletier et al., 2005). The CH basin appears as a
87 tectonic unit within the Neoproterozoic basement and it mainly consists of phyllites equilibrated
88 in greenschist-facies conditions (Ménot et al., 2005).

89 The exposed edge of the Terre Adélie Craton to the east is marked by the MSZ, which could
90 correspond to the southern extension, on the Antarctica continent, of the Kalinjila or of the
91 Coorong shear zones (Gawler Craton, south Australia) before the Cretaceous opening of the
92 Southern Ocean (Gibson et al., 2013; Talarico and Kleinschmidt, 2003b). The MSZ is several
93 km-wide, and bears a steeply-dipping pervasive mylonitic foliation and a subhorizontal to 20°
94 north-plunging lineation with predominantly dextral motion indicators (Kleinschmidt and
95 Talarico, 2000). This suggests that the MSZ might represent a mid-crustal strike-slip fault that
96 could have accommodated large horizontal displacements. Microstructural and thermo-
97 barometric studies show that the MSZ deformation likely resulted in successive shear
98 structures occurring under different metamorphic conditions from medium pressure
99 amphibolite to greenschists facies up to 1.5 Ga (Duclaux et al., 2008; Lamarque et al., 2016;
100 Talarico and Kleinschmidt, 2003b). Talarico and Kleinschmidt (2003a) highlighted undated
101 brittle structures crosscutting the mylonic foliation and Ménot et al. (2005) suggest that a
102 younger age (post-Ordovician ?) cannot be formally ruled out because Paleozoic rocks are
103 found to the East of the Mertz Glacier.

104 The domain east of the MSZ (145°E to 148°E, in yellow on Figures 1 and 2) corresponds to
105 eastern George V Land and to the Penguin-Bage-Webb block. It is characterized by outcrops
106 of granitoids with U-Pb dates of 505 Ma (Fanning et al., 2002) and $508-510 \pm 5$ Ma (Goodge
107 and Fanning, 2010). Granites from Penguin Point display a large amount of gneiss and mafic
108 microgranular xenoliths. They are massive with a mean grain size around 0.2-0.3 cm and they
109 mainly contain quartz, feldspars and large flakes of biotite. Feldspars plagioclase is more
110 abundant than K-feldspar. When compared to the descriptions of Ravich et al. (1968) given
111 for the granites from the Ainsworth Bay (now Desolation Bay), the Penguin Point granites
112 seem to be close to those of Cape Bage (located about 15 km away to East, see Figure 1) and
113 rather distinct to those of Cape Webb (more to the East, Figure 1).

114 The studied samples occur as spherical to elongated xenoliths of few tens of cm hosted within
115 the Penguin Point granite (see xenoliths description in paragraph 3)

116 **2.2/ South Australia**

117 A large part of South Australia corresponds to the Gawler Craton, which is also part of the
118 Mawson continent (Fanning et al., 2003). The Gawler Craton mainly consists of Archean to
119 Paleoproterozoic basement that is overlain and intruded by Paleoproterozoic to
120 Mesoproterozoic sedimentary, volcanic and intrusive rocks (Reid et al., 2014 and Figure 1).
121 The Archean basement is comprised of two temporally and spatially distinct pieces of crust
122 that have unrelated formation and/or metamorphic histories. Mesoarchean (*ca.* 3250-3150
123 Ma) gneisses compose the oldest rocks, which are outcropping in the southeastern Gawler
124 Craton (Reid et al., 2014, pink in Figure 1). Neoproterozoic to earliest Paleoproterozoic domains
125 include both the Sleaford Complex in the southern Gawler Craton (green in Figure 1) and the
126 Mulgathing Complex in the north central part of the craton that are composed of felsic, mafic
127 and ultramafic volcanics as well as metasedimentary lithologies representing portions of a
128 single Late Archean belt, deformed and metamorphosed during the Sleafordian Orogeny
129 between 2450 and 2420 Ma (Daly and Fanning, 1993; Swain et al., 2005). The Miltalie gneiss
130 intruded the Sleaford Complex during its uplift and erosion around 2000 Ma (Fanning et al.,
131 2007, 1988). Thereafter, the Hutchinson Group (> 1850 Ma) overlain the eastern margin of
132 the Gawler Craton (Daly and Fanning, 1993). This group includes a basal quartz-pebble
133 conglomerate and quartzite which change to calcareous and aluminous metasediments at the
134 top (Parker and Lemon, 1982). The Hutchinson Group is limited to the east by a major
135 tectonic structure, the Kalinjala shear zone (KSZ), formed during the *ca.* 1730–1690 Ma
136 Kimban Orogeny. The Kimban Orogeny completed the volcano-sedimentary basin
137 development during the Paleoproterozoic and extensively reworked the Archean and
138 Paleoproterozoic domains through the activation of transpressional shear zones, such as the

139 KSZ (Hand et al., 2007; Reid and Hand, 2012; Vassallo and Wilson, 2002). This later
140 corresponds to a 4 - 6 km wide corridor showing subvertical mylonitic structures, associated
141 magmatism as for example Middle Camp Granite and high-grade metamorphic assemblages
142 (Parker, 1980; Vassallo and Wilson, 2002). However magmatic effect of the Kimban orogeny
143 and relationships with large scale tectonic structures were mainly described across the central
144 and northern Gawler craton (Hand et al., 2007). Thermal and mechanical effects of the high-
145 strain zone activity could be observed in an area up to 100 km from the heart of the shear
146 zone (see Figure 5 of Hand et al., 2007). The KSZ likely represents a palaeosuture zone,
147 separating two crustal (or possible lithospheric-scale) blocks with compositional differences
148 (Howard et al., 2006). East of the Kalinjala shear zone, outcrops reveal the presence of a
149 small area of felsic orthogneiss basement dated at 3150 Ma and deformed around 2530-2510
150 Ma (Fraser et al., 2010). This basement did not suffer any Sleafordian deformation. The
151 Paleoproterozoic igneous Donington Suite (1850 Ma) intrudes sedimentary rocks with distinct
152 isotopic signature from those located west of the Kalinjala shear zone (Howard et al., 2009).
153 The Myola volcanics occurred between 1765 and 1735 Ma (Daly et al., 1998) and overly the
154 Donington Suite. Following the Kimban Orogeny, magmatism took place during the time
155 period 1690-1575 Ma. Markers of this magmatic activity include (i) the post-orogenic
156 intrusive Tunkillia Suite (1690-1670 Ma), which origin is still debated (Payne et al., 2010),
157 (ii) the voluminous St Peter Suite (1620-1610 Ma), which shows subduction origin (Hand et
158 al., 2007; Swain et al., 2008) (iii) the Gawler Range Volcanics (1600-1585 Ma) which
159 constitutes a silicic-dominated large igneous province (Agangi et al., 2011) and, (iv) the
160 Hiltaba Suite (1590-1575 Ma) that developed into upper-crustal syn-tectonic plutons occurring
161 in a wide zone of crustal shearing (McLean and Betts, 2003).

162 The Neoproterozoic to Paleozoic formations of South Australia are represented by the
163 Adelaide Geosyncline (Figure 1), which was fully described by Counts (2017). As a general

164 overview, this rift complex is composed by successive (super)groups defined as (i) the
165 Warrina supergroup which include both the Callanna group (minimum age around 802 ± 10
166 Ma) mainly composed of siltstone, sandstone, carbonates, evaporites and basalt; and the Burra
167 group ($\sim 777 - 700$ Ma) mainly consisting of siltstone, shale, sandstone and dolomite (Forbes
168 et al., 1981; Krieg et al., 1991), (ii) the Heysen supergroup which include both the
169 Umberatana group ($\sim 700-620$ Ma) made up of tillite, sandstone, siltstone, arkose, dolomite,
170 quartzite, conglomerate, shale and greywacke; and the Wilpena group ($\sim 588-566$ Ma) mainly
171 composed of siltstone with laminated quartzite, dolomite, marble and sandy marble (Knoll et
172 al., 2006), and, (iii) the Moralana supergroup which include, among others, the Normanville
173 ($\sim 526-515$ Ma) made of limestone; sandstone; shale and volcanics; the Kanmantoo ($\sim 522-$
174 514 Ma) including marine metasandstone, phyllite, schist, gneiss, minor calcsilicate and
175 marble; and the Lake Frome groups ($\sim 523 - 498$ Ma) composed of sandstone, siltstone,
176 shale, limestone and conglomerate (Zang et al., 2004). Study of detrital-zircon ages in the
177 Adelaide fold belt (Ireland et al., 1998) shows an abrupt change in zircon population at the
178 base of the Cambrian Kanmantoo Group. It is dominated by Ross-Delamerian ($600-500$ Ma)
179 and Grenvillean ages ($1200-1000$ Ma) whereas zircons from Neoproterozoic sedimentary
180 rocks (Normanville and older groups) mainly derived from the Australian cratons with ages
181 progressively changing from Mesoproterozoic to Neoproterozoic and only few zircon that are
182 close to the depositional age. Further east, the Murray Basin overlies these formations. The
183 outcropping Glenelg River Complex (Figure 1) as well as the Nargoon Group sampled from
184 stratigraphic drill-hole, both within the Murray Basin, were described as correlative
185 formations of Kanmantoo Group (Haines et al., 2009; Lewis et al., 2016, respectively). From
186 geophysical data, Gibson et al. (2013) defined the previously unmapped Coorong Shear zone
187 (see Figure 1). The authors proposed that the Coorong shear zone represent the correlative
188 structure of the Mertz shear zone located in Antarctica, as they are both aligned with the

189 George V Land Fracture Zone located in the Southern Ocean, thus challenging the generally
190 accepted Kalinjala-Mertz correlation (Di Vincenzo et al., 2007; Kleinschmidt and Talarico,
191 2000; Talarico and Kleinschmidt, 2003a).

192 **3/ Sample description**

193 We studied three gneiss samples hosted within the early Paleozoic granites of Penguin Point
194 (146°E), which constitutes the westernmost outcrop of granites from Penguin-Bage-Webb
195 area. The gneiss samples display sharp boundaries with the host granites (Figure 3) and
196 distinct petrographic features. Sample 12GL04 is a banded leucocratic gneiss with alternating
197 centimetric thick (up to 5 cm) quartz-feldspar layers and thin (up to 2 mm) biotite beds. It
198 could correspond to the "fine-grained feldspathic quartzite" described by Ravich et al. (1968).
199 Sample 12GL01 is a homogeneous biotite -rich gneiss. Samples 12GL01 and 12GL04 display
200 rather comparable textures and mineralogy. They mainly differ by the grain size of minerals
201 (quartz, feldspars, biotite) being larger in 12GL01 than in 12GL04. They are granoblastic to
202 grano-lepidoblastic with equigranular (0.2 to 0.3 mm-large in 12GL04 and 1.1 to 1.2 mm in
203 12GL01) undeformed quartz and feldspar mosaic suggesting a late static recrystallization
204 which would be more developed in 12GL01 compared to 12GL04. Andesine plagioclase is
205 more widely present than K-feldspar. Biotite flakes (0.2 to 1.2 mm-long) clearly mark the
206 foliation; they enclose a lot of inclusions such as zircon and Fe-oxides (mainly ilmenite).
207 Muscovite was occasionally observed.

208 Sample 12GL02 corresponds to a migmatitic gneiss with quartz-feldspar leucosomes occurring
209 as lenses and small dykelets intruding the melanocratic layers, and presenting a granular
210 texture. The melanocratic layers consist of poikiloblastic garnet crystals (up to several mm in
211 size) that contain alignments of biotite and Fe-oxides, which consist of ilmenite grains

212 generally elongated (up to 0.8mm-long and 0.4 mm-wide). Thus, biotite and ilmenite mark a
213 former foliation.

214 In all three samples, the zircon grains are mainly included within biotite crystals, but few
215 occur as intergranular isolated grains within the matrix. The high modal proportion of biotite
216 and the presence of garnet are consistent with a sedimentary origin for the protoliths, which
217 likely corresponded to greywackes.

218 **4/ U-Pb zircon data**

219 **4.1/ Analytical techniques and data processing**

220 Rock samples were crushed using standard procedure (jaw, crusher, disc mill) and sieved to
221 <500 μm . Zircon and monazite grains were separated using heavy liquids, an isodynamic
222 Frantz separator, and then handpicked under a binocular microscope to obtain a representative
223 selection of all components present in the zircon population. Selected zircon grains were
224 mounted in epoxy resin and polished to an equatorial grain section. Analytical work was
225 carried out in the Laboratoire Magmas et Volcans (Clermont-Ferrand, France). Minerals were
226 imaged by cathodoluminescence (CL) using a JEOL JSM-5910 SEM to document their
227 internal structure, resorption surfaces, and overgrowths (Hanchar and Miller, 1993; Vavra,
228 1990). The analyses involved the ablation of minerals with a Resonetics M-50 Excimer laser
229 system operating at a wavelength of 193 nm. Spot diameters of 26 μm (zircon) and 9 μm
230 (monazite) were associated to repetition rates of 3 Hz (zircon) and 1 Hz (monazite) and
231 fluency of 4.5 J/cm^2 (zircon) and 8 J/cm^2 (monazite). The ablated material was carried into
232 helium and then mixed with nitrogen and argon before injection into the plasma source of an
233 Agilent 7500cs ICP-MS (Paquette et al., 2014). The analytical method for isotope dating with
234 laser ablation ICPMS is reported in (Hurai et al., 2010; Paquette et al., 2017). Data are
235 corrected for U-Pb fractionation occurring during laser sampling and for instrumental mass

236 bias by standard bracketing with repeated measurements of GJ-1 zircon standard (Jackson et
237 al., 2004) and C83-32 monazite standard (Corfu, 1988). The occurrence of common Pb in the
238 sample was monitored by the evolution of the $^{204}\text{Pb}+\text{Hg}$ signal intensity, but no common Pb
239 correction was applied owing to the large isobaric interference from Hg. Repeated analyses of
240 91500 zircon (Wiedenbeck et al., 1995) and Trebilcock monazite (Kohn and Vervoort, 2008)
241 standards treated as unknowns yielded concordia ages of 1067 ± 3 Ma ($\text{MSWD}_{\text{(C+E)}}=0.45$;
242 $n=69$) and 271 ± 2 Ma ($\text{MSWD}_{\text{(C+E)}}=1.2$; $n=20$), independently control the reproducibility and
243 accuracy of the corrections. Data reduction was carried out with the software package
244 GLITTER[®] from Macquarie Research Ltd (Van Achterbergh et al., 2001). Calculated ratios
245 were exported and Concordia ages and diagrams were generated using Isoplot/Ex v. 3.7 Excel
246 macro package by Ludwig (2008). The concentrations in U-Th-Pb were calibrated relative to
247 the certified contents of GJ-1 zircon (Jackson et al., 2004) and Moacyr monazite (Gasquet et
248 al., 2010) standards, respectively.

249 Results of U-Pb analyses for all samples are summarized in Table 1 (supplementary data).

250 **4.2/ Results**

251 Most zircon grains analyzed in the course of this study are light yellow, but a population of
252 bigger dark brown grains was found in sample 12GL02, some of which being metamict.

253 Cathodoluminescence images of representative grains are presented in Figure 4. They are
254 characterized by elliptical to rounded shapes (aspect ratio ranging from 0.3 to 1 with mean
255 value of about 0.6). Core-rim relationships are common and most core and rim domains
256 feature oscillatory to patchy zoning. Narrow CL-bright rims ($<10 \mu\text{m}$ large) are also observed.

257 Secondary textures include healed cracks and fractures. In some cases, only part of the zircon
258 grain is preserved and do not show any core-rim structure. The variety of internal growth
259 structures and the wide range of Th/U ratios between 0.01 and 5.78 support derivation from

260 various igneous and/or metamorphic protoliths, consistent with a metasedimentary origin of
261 the gneiss samples.

262 Results of zircon U-Pb dating are presented in Wetherill diagrams for each sample in Figure
263 5a,b and 6a. Zircon date distributions are reported as Kernel Density Estimates (Fig. 5e,f)
264 following Vermeesch(2012). The comprehensive analytical dataset for all grains is provided
265 in Table S1 (supplementary data). In the following, quoted dates are $^{206}\text{Pb}/^{238}\text{U}$ dates when
266 younger than 1.2 Ga. Otherwise, the $^{207}\text{Pb}/^{206}\text{Pb}$ dates are preferred.

267 **Sample 12GL02**

268 A total of 76 U-Pb analyses were performed on 62 zircon grains. Sixty-two analyses are
269 concordant at 90 – 110 % (with concordance defined as $^{206}\text{Pb}/^{238}\text{U}$ date / $^{207}\text{Pb}/^{206}\text{Pb}$ date x
270 100). Following Vermeesch (2004), it entails that we can be confident at 95% that no fraction
271 representing more than 8% of the sample has been missed. 12GL02 is typified by (i) a
272 dominant Ediacaran (549-628 Ma) zircon population (N=27; Fig. 5a,c); (ii) a subordinate
273 population (N=4) with Cryogenian-late Tonian dates (693-784 Ma); (iii) grains yielding dates
274 scattered between the early Tonian and the Stenian (0.9 to 1.2 Ga; N=10); (iv) an important
275 Archean population (N=21), clustering at c. 2.7 and 3.1 Ga (Fig. 5c). Besides, four discordant
276 analyses show $^{207}\text{Pb}/^{206}\text{Pb}$ dates in excess of 2.6 Ga. Importantly, zircon grains showing
277 Ediacaran and Archean dates display a very large range of Th/U ratios (from 0.01 to 2.39,
278 Tab. S1) and textural patterns. In contrast, the early Tonian-Stenian population mostly
279 consists of grains with oscillatory zoning textures and elevated Th/U ratios (mostly between
280 0.3 and 0.8, Tab. S1). The 16 youngest Ediacaran grains showing overlapping $^{206}\text{Pb}/^{238}\text{U}$ dates
281 at 2σ allowed calculation of a weighted average date of 569.4 ± 5.0 Ma (Fig. 5e). Finally, one
282 single CL-dark, low Th/U (0.03) and U-rich (2600 ppm) zircon crystal yielded a Cambrian
283 $^{206}\text{Pb}/^{238}\text{U}$ date of 514 ± 18 Ma.

284 **Sample 12GL04**

285 Thirty-four measurements were performed on 27 zircon grains and 23 yielded U-Pb dates
286 concordant at 90–110%, meaning that no fraction representing more than 18% of the sample
287 has been missed (at 95% confidence). Sample 12GL04 also features a dominant Ediacaran
288 population (569–622 Ma, N=9, Fig. 5b,d) with again a large variety of internal growth
289 structures and a wide range of Th/U ratios between 0.11 and 5.78 (Tab. S1). Two grains
290 yielded Tonian dates of 848 ± 29 and 910 ± 31 Ma. One grain show a date of 1200 ± 40 Ma,
291 i.e. at the Stenian-Ectasian boundary. Notably, 12GL04 differs from 12GL02 by the presence
292 of a Paleoproterozoic zircon population defining sub peaks at c. 1.9 and 2.4 Ga (N=5). Grains
293 of that age feature oscillatory zoning patterns and a narrow range of Th/U ratios (0.33 to 0.52,
294 Tab. S1). One grain has the oldest concordant $^{207}\text{Pb}/^{206}\text{Pb}$ date retrieved in the course of this
295 study (at 3.4 Ga). Finally, a weighted average date of 575.2 ± 8.3 Ma can be calculated
296 considering the 6 youngest Ediacaran grains showing overlapping $^{206}\text{Pb}/^{238}\text{U}$ dates at 2σ (Fig.
297 5f).

298 **Sample 12GL01**

299 Only 15 zircon grains were extracted from this sample and 16 U-Pb analyses were performed
300 out of which 9 are concordant at 90–110%. Two grains show Ediacaran dates of 575 ± 21 and
301 633 ± 22 Ma. Three grains yielded Stenian-late Ectasian dates (at 1.1–1.2 Ga) and four grains
302 Archean dates spanning between 2.6 and 3.3 Ga. In addition, 7 monazite grains were also
303 retrieved from this sample. Seven out of 8 analyses are equivalent (Fig. 6b) and allow
304 calculation of a robust Concordia date at 514.6 ± 5.2 Ma ($\text{MSWD}_{(\text{C+E})} = 1.07$).
305 notably, when all three samples are considered together, zircon date distributions evidence a
306 tendency toward younger ages for the rims (blue) and older ages for the cores (red), both
307 populations recording similar age patterns (Fig. 7).

308 **5/ Discussion**

309 **5.1. Interpretation of the U-Pb results**

310 As the investigated xenoliths are interpreted to be metasediments, the new U-Pb dataset can
311 place constraints on the maximal depositional ages of the sedimentary protoliths. Those were
312 calculated based on the robust YC2 σ (3+) estimator of Dickinson and Gehrels (2009), i.e. the
313 weighted mean age of the youngest zircon population of at least three grains showing
314 overlapping $^{206}\text{Pb}/^{238}\text{U}$ dates at 2σ . This approach is particularly suited in the absence of
315 distinctive correlations between zircon date and U content or Th/U ratios, as observed among
316 the Ediacaran populations of samples 12GL02 and 12GL04. Calculated maximal depositional
317 ages are 569.4 ± 5.0 Ma and 575.2 ± 8.3 Ma, respectively (Fig. 5c,d). No depositional age was
318 obtained for 12GL01 as only 2 Ediacaran dates were retrieved and do not overlap (Fig. 6a).
319 As the enclosing granites are ca. 505 Ma-old, the protoliths of the paragneiss xenoliths are
320 unambiguously of Ediacaran – Lower Cambrian age.

321 The monazite date of 514.6 ± 5.2 Ma most probably constrains the timing of metamorphism
322 experienced by the xenoliths, before incorporation in the granitic magmas. This age is
323 identical to the Cambrian $^{206}\text{Pb}/^{238}\text{U}$ date of 514 ± 18 Ma measured on a zircon grain from
324 sample 12GL02, suggesting that this grain possibly (re)crystallized or got its U-Pb system
325 reset during high-grade metamorphism, in agreement with its low Th/U ratio of 0.03 (Rubatto
326 et al., 2001). Metamorphism and plutonic activity at 515-500 Ma can be related to the Ross
327 orogeny (Boger, 2011) which affected several segments of Antarctica and Australia. In that
328 sense, the paragneiss xenoliths of eastern George V Land most probably represent relics of
329 the paleo-Pacific margin of eastern Gondwana that was deformed and metamorphosed during
330 the Ross orogeny.

331 **5.2/ Relationships between the PBW block and the Terre Adélie-Gawler Cratons**

332 U/Pb ages in the Terre Adélie Craton Paleoproterozoic domain have been published by Peucat
333 et al. (1999). They show (i) that the Dumont d'Urville basin contains two populations of
334 inherited zircon grains bearing SHRIMP ages of about 1.73-1.76, 2.6 and 2.8 Ga and (ii) that
335 a major partial melting event, marked by newly formed zircon and monazite grains, occurred
336 at around 1.69 Ga. In the Neoproterozoic domain of the Terre Adélie Craton, U-Pb ages were
337 obtained by Oliver et al. (1983); Oliver and Fanning (2002); Ménot (in press). They range
338 between 2.4 and 2.5 Ga and indicate a major period of magmatism and of high grade
339 metamorphism.

340 Importantly, there is a clear mismatch between the ages recorded in the Terre Adélie craton
341 and the zircon U-Pb date distribution of paragneisses from the PBW block (Figure 8). In the
342 latter, grains with dates between 1.6 and 1.8 Ga are lacking and only 4 grain domains show
343 dates in the range 2.4 – 2.6 Ga. A similar conclusion can be drawn when the Gawler craton is
344 considered (Fig. 8). These results clearly indicate that the source of older-than-1 Ga zircon
345 grains in the Ediacaran – Lower Cambrian detritus does not originate from the Terre
346 Adélie/Gawler craton. In terms of geodynamic reconstruction, it implies that either (i) an old
347 basement similar to the Terre Adélie/Gawler Cratons is present beneath the PBW block but
348 was not exposed at the time of sediment deposition (Ediacaran to Lower Cambrian) so that it
349 was not reworked as detritus feeding the Ediacaran-Lower Cambrian basins, or (ii) the lack of
350 Terre Adélie/Gawler Cratons signature reflects the presence of a different basement in the
351 PBW block. We favor the second hypothesis because seismic investigations (Lamarque et al.,
352 2015), aeromagnetic exploration (Aitken et al., 2014; Ferraccioli et al., 2009; Finn et al.,
353 2006) and gravity data (Jordan et al., 2013) support that the MSZ is a major continental scale
354 tectonic structure that clearly separates two distinct lithospheric domains of probably
355 contrasted ancestries.

356 **5.3. Correlations with South Australia**

357 In order to better constrain the relationships between Antarctica and South Australia before
358 the opening of the Southern Ocean, we attempt to identify the correlative formation(s) of our
359 samples in South Australia. We thus compare in Figure 9 the detrital zircon U-Pb age
360 distribution of Penguin Point paragneisses to those of the Kanmantoo, Normanville,
361 Adelaidian and Nargoon (meta)sedimentary formations, all deposited in the Ediacaran to
362 Lower Cambrian. From a graphical observation (Fig. 9), the zircon U-Pb date distribution of
363 eastern George V Land paragneisses clearly resembles that of the Kanmantoo and Nargoon
364 group sediments. Indeed, they are all characterized by a dominant Ediacaran (≈ 550 -630 Ma)
365 zircon population which is notably lacking in the of Normanville and Adelaidian formations
366 (Fig. 9). The latter instead encompass a prominent Mesoproterozoic zircon population not
367 observed in our samples. The match between PBW paragneisses and Kanmantoo/Nargoon
368 sediments is not perfect as: (i) Tonian-Stenian zircon grains are rather scarce in PBW but
369 common to abundant in the Kanmantoo/Nargoon sediments; (ii) the peak at ca. 2.7 Ga typical
370 of the PBW paragneisses is lacking in the Kanmantoo/Nargoon sediments. Because they are
371 of same age (Ediacaran to Lower Cambrian), present a similar zircon date distribution and are
372 (at least for PBW and Kanmantoo) intruded by Paleozoic granitoids formed during the Ross-
373 Delamerian orogeny (see Figure 1, Di Vincenzo et al., 2007; Foden et al., 2002), we regard
374 the PBW paragneisses as being lateral equivalents to the Kanmantoo/Nargoon sedimentary
375 formations. The above-mentioned discrepancies between their U-Pb date distributions likely
376 reflect lateral variations in the nature of the detritus.

377

378 **6/ Conclusion**

379 Zircon and monazite U-Pb dating of paragneisses from the eastern George V Land region
380 reinforces the geological correlations between South Australia and the Terre Adélie-George V
381 Land regions and support the previous geodynamical reconstructions, which were synthesized
382 by Boger (2011). In particular, we have shown that:

383 (i) Zircon and monazite ages suggest that the studied gneisses are relics of the pre-Gondwana
384 margin, which had been deformed and metamorphosed during the early Paleozoic Ross
385 orogeny.

386 (ii) Zircon date distributions of the studied samples present strong similarities with the
387 Ediacaran to Lower Cambrian Kanmantoo and Nargoon groups of South Australia, arguing
388 for a correlation between these formations. This has implications for correlations between the
389 east Mertz Shear Zone area in East Antarctica and the eastern terrains of the Gawler Craton in
390 South Australia before the opening of the Southern Ocean.

391 (iii) There is a clear mismatch between the date distribution of older-than-Mesoproterozoic
392 zircon grains recovered from the paragneisses and the geological record of the adjacent Terre
393 Adélie (and Gawler) cratons. This observation brings into question the actual source of the
394 Paleoproterozoic to Archean detritus that fed the Ediacaran to Lower Cambrian basins of the
395 PBW domain.

396 **Acknowledgements**

397 This work was supported by the French Polar Institute (IPEV, Institut Paul Emile Victor)
398 through the programme ArLiTA (Architecture de la Lithosphère de Terre Adélie). ArLiTA
399 also benefited of the support of the INSU-SYSTER programme. This work was also
400 supported by the "Laboratoire d'Excellence" LabexMer (ANR-10-LABX-19) and co-funded
401 by a grant from the French government under the program "Investissements d'Avenir", and by

402 a grant from the Regional Council of Brittany (SAD program). Thanks are due to Steven
403 Boger, John Goodge and an anonymous reviewer for their constructive reviews that permit us
404 to greatly improve the document.

405 **Bibliography**

406 Agangi, A., McPhie, J., Kamenetsky, V.S., 2011. Magma chamber dynamics in a silicic LIP
407 revealed by quartz: The Mesoproterozoic Gawler Range Volcanics. *Lithos* 126, 68–83.
408 doi:10.1016/j.lithos.2011.06.005

409 Aitken, A.R.A., Young, D.A., Ferraccioli, F., Betts, P.G., Greenbaum, J.S., Richter, T.G.,
410 Roberts, J.L., Blankenship, D.D., Siegert, M.J., 2014. The subglacial geology of Wilkes
411 Land, East Antarctica. *Geophysical Research Letters* 41, 2390–2400.
412 doi:10.1002/2014GL059405

413 Boger, S.D., 2011. Antarctica — Before and after Gondwana. *Gondwana Research* 19, 335–
414 371. doi:10.1016/j.gr.2010.09.003

415 Borg, S.G., DePaolo, D.J., 1994. Laurentia, Australia, and Antarctica as a Late Proterozoic
416 supercontinent : Constraints from isotopic mapping. *Geology* 22, 307–310.

417 Corfu, F., 1988. Differential response of U-Pb systems in coexisting accessory minerals,
418 Winnipeg River Subprovince, Canadian Shield: implications for Archean crustal growth
419 and stabilization. *Contributions to Mineralogy and Petrology* 98, 312–325.
420 doi:10.1007/BF00375182

421 Counts, J.W., 2017. The Adelaide Rift Complex in the Flinders Ranges : Geologic history ,
422 past investigations and relevant analogues The Adelaide Rift Complex in the Flinders
423 Ranges : Geologic history , past investigations and relevant analogues.
424 doi:10.13140/RG.2.2.23216.25609

- 425 Daly, S.J., Fanning, C.M., Fairclough, M.C., 1998. Tectonic evolution and exploration
426 potential of the Gawler Craton, South Australia. *Journal of Australian Geology and*
427 *Geophysique* 17, 145–168.
- 428 Daly, S.J., Fanning, C.M., 1993. Archaean., in: Drexel, J.F., Preiss, W.V., Parker, A.J. (Eds.),
429 *The Geology of South Australia, The Precambrian, Vol. 1., Bulletin 54., Geological*
430 *Survey of South Australia, Adelaide, South Australia, pp. 32–49.*
- 431 Di Vincenzo, G., Grande, A., Rossetti, F., 2014. Paleozoic siliciclastic rocks from northern
432 Victoria Land (Antarctica): Provenance, timing of deformation, and implications for the
433 Antarctica-Australia connection. *Geological Society of America Bulletin.*
434 doi:10.1130/B31034.1
- 435 Di Vincenzo, G., Talarico, F., Kleinschmidt, G., 2007. An $^{40}\text{Ar}/^{39}\text{Ar}$ investigation of the
436 Mertz Glacier area (George V Land, Antarctica): Implications for the Ross Orogen–East
437 Antarctic Craton relationship and Gondwana reconstructions. *Precambrian Research* 152,
438 93–118. doi:10.1016/j.precamres.2006.10.002
- 439 Dickinson, W.R., Gehrels, G.E., 2009. Use of U-Pb ages of detrital zircons to infer maximum
440 depositional ages of strata: A test against a Colorado Plateau Mesozoic database. *Earth*
441 *and Planetary Science Letters* 288, 115–125. doi:10.1016/j.epsl.2009.09.013
- 442 Duclaux, G., Rolland, Y., Ruffet, G., Ménot, R.-P., Guillot, S., Peucat, J.-J., Fanning, M.,
443 Rey, P., Pêcher, A., 2008. Superimposed Neoproterozoic and Paleoproterozoic tectonics in
444 the Terre Adélie Craton (East Antarctica): Evidence from Th–U–Pb ages on monazite
445 and $^{40}\text{Ar}/^{39}\text{Ar}$ ages. *Precambrian Research* 167, 316–338.
446 doi:10.1016/j.precamres.2008.09.009
- 447 Fanning, C., Ménot, R.P., Peucat, J., Pelletier, A., 2002. A closer examination of the direct
448 links between Southern Australia and Terre Adélie and George V Land, Antarctica, in:

449 16th Australian Geological Convention. Adelaide.

450 Fanning, C., Moore, D.H., Bennett, V., Daly, S., Ménot, R.P., Peucat, J., Oliver, R., 1999.

451 The “Mawson Continent” : The East Antarctic Shield and Gawler Craton, Australia, in:

452 8th International Symposium on Antarctic Earth Sciences, Wellington (New Zealand). p.

453 103.

454 Fanning, C.M., Flint, R.B., Parker, A.J., Ludwig, K.R., Blissett, A.H., 1988. Refined

455 Proterozoic Evolution of the Gawler, south Australia, through U-Pb zircon

456 geochronology. *Precambrian Research* 41, 363–386.

457 Fanning, C.M., Peucat, J.J., Ménot, R.P., 2003. Whither the Mawson continent?, in: 9th

458 International Symposium on Antarctic Earth Sciences. Potsdam.

459 Fanning, C.M., Reid, A.J., Teale, G.S., 2007. A geochronological framework for the Gawler

460 Craton, South Australia. *South Australia Geological Survey Bulletin*.

461 Ferraccioli, F., Armadillo, E., Jordan, T., Bozzo, E., Corr, H., 2009. Aeromagnetic

462 exploration over the East Antarctic Ice Sheet: A new view of the Wilkes Subglacial

463 Basin. *Tectonophysics* 478, 62–77. doi:10.1016/j.tecto.2009.03.013

464 Finn, C.A., Goodge, J.W., Damaske, D., Fanning, C.M., 2006. Scouting craton’s edge in

465 paleo-Pacific Gondwana, in: *Antarctica : Contributions to Global Earth Sciences*. Berlin

466 Heidelberg New York, pp. 165–174.

467 Fitzsimons, I.C.W., 2003. Proterozoic basement provinces of southern and southwestern

468 Australia, and their correlation with Antarctica. *Geological Society, London, Special*

469 *Publications* 206, 93–130. doi:10.1144/GSL.SP.2003.206.01.07

470 Flöttmann, T., Gibson, G.M., Kleinschmidt, G., 1993. Structural continuity of the Ross and

471 Delamerian orogens of Antarctica and Australia along the margin of the paleo-Pacific.

472 *Geology* 21, 319–322.

473 Foden, J.D., Elburg, M.A., Turner, S.P., Sandiford, M., O'Callaghan, J., Mitchell, S., 2002.
474 Granite production in the Delamerian Orogen, South Australia. *Journal of the Geological*
475 *Society* 159, 557–575. doi:10.1144/0016-764901-099

476 Forbes, B.G., Murrell, B., Preiss, W.V., 1981. Subdivision of Lower Adelaidean Willouran
477 Ranges.

478 Fraser, G., McAvaney, S., Neumann, N., Szpunar, M., Reid, A., 2010. Discovery of early
479 Mesoarchean crust in the eastern Gawler Craton, South Australia. *Precambrian Research*
480 179, 1–21. doi:10.1016/j.precamres.2010.02.008

481 Gasquet, D., Bertrand, J., Paquette, J., Lehmann, J., Ratzov, G., De Ascensão Guedes, R.,
482 Tiepolo, M., Boullier, A., Scaillet, S., Nomade, S., 2010. Miocene to Messinian
483 deformation and hydrothermalism in the Lauzière Massif (French Western Alps): New
484 U-Th-Pb and Argon ages. *Bulletin de la Societe Geologique de France* 181, 227–241.

485 Gibson, G.M., Totterdell, J.M., White, L.T., Mitchell, C.H., Stacey, A.R., Morse, M.P.,
486 Whitaker, A., 2013. Pre-existing basement structure and its influence on continental
487 rifting and fracture zone development along Australia's southern rifted margin. *Journal*
488 *of the Geological Society* 170, 365–377. doi:10.1144/jgs2012-040

489 Goodge, J.W., Fanning, C.M., 2010. Composition and age of the East Antarctic Shield in
490 eastern Wilkes Land determined by proxy from Oligocene-Pleistocene glaciomarine
491 sediment and Beacon Supergroup sandstones, Antarctica. *Geological Society of America*
492 *Bulletin* 122, 1135–1159. doi:10.1130/B30079.1

493 Haines, P.W., Turner, S.P., Foden, J.D., Jago, J.B., 2009. Isotopic and geochemical
494 characterisation of the Cambrian Kanmantoo Group, South Australia: implications for
495 stratigraphy and provenance. *Australian Journal of Earth Sciences* 59, 1095–1110.

496 Hanchar, J.M., Miller, C.F., 1993. Zircon zonation patterns as revealed by

497 cathodoluminescence and backscattered electron images: Implications for interpretation
498 of complex crustal histories. *Chemical Geology* 110, 1–13. doi:10.1016/0009-
499 2541(93)90244-D

500 Hand, M., Reid, A., Jagodzinski, L., 2007. Tectonic Framework and Evolution of the Gawler
501 Craton, Southern Australia. *Economic Geology* 102, 1377–1395.
502 doi:10.2113/gsecongeo.102.8.1377

503 Howard, K.E., Hand, M., Barovich, K.M., Reid, A., Wade, B.P., Belousova, E. a., 2009.
504 Detrital zircon ages: Improving interpretation via Nd and Hf isotopic data. *Chemical*
505 *Geology* 262, 293–308. doi:10.1016/j.chemgeo.2009.01.029

506 Howard, K.E., Reid, a. J., Hand, M.P., Barovich, K.M., Belousova, E. a., 2006. Does the
507 Kalinjala Shear Zone represent a palaeosuture zone ? Implications for distribution of
508 styles of Mesoproterozoic mineralisation in the Gawler Craton. *Earth* 16–20.

509 Hurai, V., Paquette, J.L., Huraiová, M., Konečný, P., 2010. U-Th-Pb geochronology of zircon
510 and monazite from syenite and pincinite xenoliths in Pliocene alkali basalts of the intra-
511 Carpathian back-arc basin. *Journal of Volcanology and Geothermal Research* 198, 275–
512 287. doi:10.1016/j.jvolgeores.2010.09.012

513 Ireland, T.R., Flöttmann, T., Fanning, C.M., Gibson, G.M., Preiss, W. V., 1998. Development
514 of the early Paleozoic Pacific margin of Gondwana from detrital-zircon ages across the
515 Delamerian orogen. *Geology* 26, 243–246. doi:10.1130/0091-7613(1998)026<0243

516 Jackson, S.E., Pearson, N.J., Griffin, W.L., Belousova, E.A., 2004. The application of laser
517 ablation-inductively coupled plasma-mass spectrometry to in situ U-Pb zircon
518 geochronology. *Chemical Geology* 211, 47–69. doi:10.1016/j.chemgeo.2004.06.017

519 Jordan, T.A., Ferraccioli, F., Armadillo, E., Bozzo, E., 2013. Crustal architecture of the
520 Wilkes Subglacial Basin in East Antarctica, as revealed from airborne gravity data.

521 Tectonophysics 585, 196–206. doi:10.1016/j.tecto.2012.06.041

522 Kleinschmidt, G., Talarico, F., 2000. The Mertz Shear Zone. *Terra Antarctica Reports* 5, 109–
523 115.

524 Knoll, A.H., Walter, M.R., Narbonne, G.M., Christie-Blick, N., 2006. The Ediacaran period:
525 A new addition to the geologic time scale. *Lethaia* 39, 13–30.
526 doi:10.1080/00241160500409223

527 Kohn, M.J., Vervoort, J.D., 2008. U-Th-Pb dating of monazite by single-collector ICP-MS:
528 Pitfalls and potential. *Geochemistry, Geophysics, Geosystems* 9.
529 doi:10.1029/2007GC001899

530 Krieg, G.W., Rogers, P.A., Callen, R.A., Freeman, P.J., Alley, N.F., Forbes, B.G., 1991.
531 Curdimurka, South Australia.

532 Lamarque, G., Barruol, G., Fontaine, F.R., Bascou, J., Ménot, R.-P., 2015. Crustal and mantle
533 structure beneath the Terre Adelie Craton, East Antarctica: insights from receiver
534 function and seismic anisotropy measurements. *Geophysical Journal International* 200,
535 809–823. doi:10.1093/gji/ggu430

536 Lamarque, G., Bascou, J., Maurice, C., Cottin, J.-Y., Riel, N., Ménot, R.-P., 2016.
537 Microstructures, deformation mechanisms and seismic properties of a Palaeoproterozoic
538 shear zone: The Mertz shear zone, East-Antarctica. *Tectonophysics* 680, 174–191.
539 doi:10.1016/j.tecto.2016.05.011

540 Lewis, C.J., Cayley, R.A., R.J., D., Schofield, A., Taylor D.H., 2016. New SHRIMP U-Pb
541 zircon ages from the Stavely region, western Victoria: July 2014-June 2016, *Geoscience*
542 *Australia*.

543 Ludwig, K., 2008. User's manual for Isoplot Version 3.70, a geochronological toolkit for
544 Microsoft Excel. *Berkeley Geochronology Center Special Publications* 4, 1–76.

545 McLean, M.A., Betts, P.G., 2003. Geophysical constraints of shear zones and geometry of the
546 Hiltaba Suite granites in the western Gawler Craton, Australia. *Australian Journal of*
547 *Earth Sciences* 50, 525–541. doi:10.1046/j.1440-0952.2003.01010.x

548 Ménot, R.-P., n.d. East Antarctica, in: G. Kleinschmidt Ed., Schweizerbart'sche Verlags,
549 Stuttgart, D. (Ed.), *Geology of the Antarctic Continent*.

550 Ménot, R., Pêcher, A., Rolland, Y., Peucat, J., Pelletier, A., Duclaux, G., Guillot, S., 2005.
551 Structural Setting of the Neoproterozoic Terrains in the Commonwealth Bay Area (143-
552 145°E), Terre Adélie Craton, East Antarctica. *Gondwana Research* 8, 1–9.

553 Ménot, R.P., n.d. East Antarctica, in: Kleinschmidt, G. (Ed.), *Geology of the Antarctic*
554 *Continent*. Schweizerbart Plut, Stuttgart.

555 Ménot, R.P., Duclaux, G., Peucat, J.J., Rolland, Y., Guillot, S., Fanning, M., Bascou, J.,
556 Gapais, D., Pêcher, A., 2007. Geology of the Terre Adélie Craton (135 – 146°E), East
557 Antarctica, in: Cooper, A., Raymond, C., Al., E. (Eds.), *Antarctica: A Keystone in a*
558 *Changing World - Online Proceedings for the Tenth International Symposium on*
559 *Antarctica Earth Sciences*. USGS Open-file Report 2007-1047, extended Abstract, p.
560 1047. doi:10.3133/of2007-1047.srp048

561 Milnes, A.R., Compston, W., Daily, B., 1977. Pre- to syn-tectonic emplacement of early
562 palaeozoic granites in southeastern south Australia. *Journal of the Geological Society of*
563 *Australia* 24, 87–106.

564 Oliver, R., Cooper, J.A., Truelove, A.J., 1983. Petrology and zircon geochronology of Herring
565 Island and Commonwealth Bay and Evidence for Gondwana Reconstruction, in:
566 *Antarctic Earth Science*. pp. 64–68.

567 Oliver, R., Fanning, C., 2002. Proterozoic geology east and southeast of Commonwealth Bay,
568 George V Land, Antarctica, and its relationship to that of adjacent Gondwana terranes,

569 in: Antarctica at the Close of the Millenium. Royal Society of New Zealand, Bulletin 35,
570 51-58.

571 Oliver, R., Fanning, C., 1997. Australia and Antarctica : Precise correlation of
572 Paleoproterozoic terrains, in: The Antarctic Region : Geological Evolution and
573 Processes. pp. 163–172.

574 Paquette, J.L., Ballèvre, M., Peucat, J.J., Cornen, G., 2017. From opening to subduction of an
575 oceanic domain constrained by LA-ICP-MS U-Pb zircon dating (Variscan belt, Southern
576 Armorican Massif, France). *Lithos* 294–295, 418–437. doi:10.1016/j.lithos.2017.10.005

577 Paquette, J.L., Piro, J.L., Devidal, J.L., Bosse, V., Didier, A., 2014. Sensitivity enhancement
578 in LA-ICP-MS by N2 addition to carrier gas : application to radiometric dating of U-Th-
579 bearing minerals. *Agilent ICP-MS journal* 58, 4–5.

580 Parker, A.J., Lemon, N.M., 1982. Reconstruction of the Early Proterozoic stratigraphy Of the
581 Gawler Craton, South Australia. *Journal of the Geological Society of Australia* 29, 221–
582 238. doi:10.1080/00167618208729206

583 Payne, J.L., Ferris, G., Barovich, K.M., Hand, M., 2010. Pitfalls of classifying ancient
584 magmatic suites with tectonic discrimination diagrams: An example from the
585 Paleoproterozoic Tunkillia Suite, southern Australia. *Precambrian Research* 177, 227–
586 240. doi:10.1016/j.precamres.2009.12.005

587 Payne, J.L., Hand, M., Barovich, K.M., Reid, A., Evans, D.A.D., 2009. Correlations and
588 reconstruction models for the 2500-1500 Ma evolution of the Mawson Continent.
589 Geological Society, London, Special Publications 323, 319–355. doi:10.1144/SP323.16

590 Pelletier, A., Guiraud, M., Menot, R.-P., 2005. From partial melting to retrogression in the
591 Pointe Geologie migmatitic complex: a history of heterogeneous distribution of fluids.
592 *Lithos* 81, 153–166. doi:10.1016/j.lithos.2004.10.003

593 Peucat, J.J., Capdevila, R., Fanning, C.M., Ménot, R.P., Pécora, L., Testut, L., 2002. 1.60 Ga
594 felsic volcanic blocks in the moraines of the Terre Adélie Craton, Antarctica :
595 comparisons with the Gawler Range Volcanics, South Australia. *Australian Journal of*
596 *Earth Sciences* 49, 831–845.

597 Peucat, J.J., Ménot, R.P., Monnier, O., Fanning, C., 1999. The Terre Adélie basement in the
598 East-Antarctica Shield : geological and isotopic evidence for a major 1.7 Ga thermal
599 event ; comparison with the Gawler Craton in South Australia. *Precambrian Research* 94,
600 205–224.

601 Ravich, M.G., Klimov, L. V., Solov'ev, D.S., 1968. The Pre-Cambrian of the East Antarctica.
602 Isreal Program for Scientific Translations Ltd (translation of Ravich et al., 1965),
603 Jerusalem.

604 Reading, A.M., 2004. The Seismic Structure of Wilkes Land/Terre Adélie, East Antarctica
605 and Comparison with Australia: First Steps in Reconstructing the Deep Lithosphere of
606 Gondwana. *Gondwana Research* 7, 21–30. doi:10.1016/S1342-937X(05)70303-8

607 Reid, A.J., Hand, M., 2012. Mesoarchean to Mesoproterozoic evolution of the southern
608 Gawler Craton, South Australia. *Episodes* 35, 216–225.

609 Reid, A.J., Jagodzinski, E. a., Armit, R.J., Dutch, R. a., Kirkland, C.L., Betts, P.G., Schaefer,
610 B.F., 2014. U-Pb and Hf isotopic evidence for Neoproterozoic and Paleoproterozoic
611 basement in the buried northern Gawler Craton, South Australia. *Precambrian Research*
612 250, 127–142. doi:10.1016/j.precamres.2014.05.019

613 Rubatto, D., Williams, I.S., Buick, I.S., 2001. Zircon and monazite response to prograde
614 metamorphism in the Reynolds Range, central Australia. *Contributions to Mineralogy*
615 *and Petrology* 140, 458–468. doi:10.1007/PL00007673

616 Swain, G., Hand, M., Teasdale, J., Rutherford, L., Clark, C., 2005. Age constraints on terrane-

617 scale shear zones in the Gawler Craton, southern Australia. *Precambrian Research* 139,
618 164–180. doi:10.1016/j.precamres.2005.06.007

619 Talarico, F., Kleinschmidt, G., 2003a. The Mertz Shear Zone (George V Land): Implications
620 for Australia/Antarctica Correlations and East Antarctic Craton/Ross Orogen
621 Relationships. *Terra Antarctica Reports* 9, 149–153.

622 Talarico, F., Kleinschmidt, G., 2003b. Structural and metamorphic evolution of the Mertz
623 Shear Zone (East Antarctic Craton, George V Land) : implications for
624 Australia/Antarctica correlations and East Antarctic craton/Ross orogen relationships.
625 *Terra Antarctica* 10, 229–248.

626 Van Achterbergh, E., Ryan, C., Jackson, S., Griffin, W., 2001. Data reduction software for
627 LA-ICP-MS, in: *Laser Ablation-ICPMS in the Earth Science*. Mineralogical Association
628 of Canada., pp. 239–243.

629 Vassallo, J.J., Wilson, C.J.L., 2002. Palaeoproterozoic regional-scale non-coaxial
630 deformation: an example from eastern Eyre Peninsula, South Australia. *Journal of*
631 *Structural Geology* 24, 1–24. doi:10.1016/S0191-8141(01)00043-8

632 Vavra, G., 1990. On the kinematics of zircon growth and its petrogenetic significance: a
633 cathodoluminescence study. *Contributions to Mineralogy and Petrology* 106, 90–99.
634 doi:10.1007/BF00306410

635 Vermeesch, P., 2013. Multi-sample comparison of detrital age distributions. *Chemical*
636 *Geology* 341, 140–146. doi:10.1016/j.chemgeo.2013.01.010

637 Vermeesch, P., 2012. On the visualisation of detrital age distributions. *Chemical Geology*
638 312–313, 190–194. doi:10.1016/j.chemgeo.2012.04.021

639 Wiedenbeck, M., Allé, P., Corfu, F., Griffin, W.L., Meier, M., Oberli, F., Quadt, A. VON,
640 Roddick, J.C., Spiegel, W., 1995. Three Natural Zircon Standards for U-Th-Pb, Lu-Hf,

641 Trace Element and Ree Analyses. *Geostandards and Geoanalytical Research* 19, 1–23.

642 doi:10.1111/j.1751-908X.1995.tb00147.x

643

644 **Figure captions**

645 **Figure 1:** A/ General map of Antarctica and Australia. B/ Simplified geological map of the
646 Gawler Craton and juxtaposed terrains (modified from Foden et al., 2002; Haines et al., 2009;
647 Howard et al., 2006; Milnes et al., 1977; Reid et al., 2014). C/ Synthetic geological map of
648 study area, modified from Ménot et al. (2005). The green area represents the Terre Adélie
649 Craton, whereas the yellow area is related to the Ross orogeny. The red circle represents the
650 studied outcrop (Penguin Point). Note that the geological maps of south Australia and Terre
651 Adélie-George V Land (B and C) are juxtaposed for graphical purpose but this is not
652 representative of any paleo-reconstruction.

653 **Figure 2:** **A:** Location of Terre Adélie and George V Land in the Antarctic continent. **B:** Link
654 between south Australia and Antarctica. TAC = Terre Adélie Craton, GC = Gawler Craton,
655 MSZ = Mertz shear zone, KSZ = Kalinjala shear zone, CSZ = Coorong shear zone. **C:**
656 Synthetic geological map of the Terre Adélie Craton (after Ménot et al., 2007). Purple areas
657 are Paleoproterozoic terrains, which correspond to the Dumont d'Urville and Cape Hunter
658 basins; green and brown areas are Neoproterozoic terrains, green being intermediate to upper
659 amphibolitic crust and brown granulite facies crust. Orange area represents the Paleozoic
660 crust, mainly composed of granitoids. Darkest colours correspond to outcrops. MSZ denotes
661 the Mertz shear zone and ZSZ denotes the Zélée shear zone. Directions of field-measured
662 structures are drawn in black. Locations of studied samples are marked by red stars. See also
663 Ménot et al. (2007) and Ménot (to be published) for more complete geological description.

664 **Figure 3:** A, B/ Photographs of xenoliths in the field, and their relations with the host granite.
665 C/ Thin-section photograph of sample 12GL01. D, E/ Thin-section photograph of sample
666 12GL02. F/ Thin-section photograph of sample 12GL04.

667 **Figure 4:** Cathodoluminescence images of selected zircon grains from paragneiss
668 xenoliths 12GL01, 12GL02 and 12-GL04. The circles represent the locations of laser spots

669 and the obtained dates (in Ma) together with their uncertainties (at 2σ). $^{206}\text{Pb}/^{238}\text{U}$ dates are
670 reported when younger than 1.2 Ga. For older dates, the $^{207}\text{Pb}/^{206}\text{Pb}$ dates are preferred. This
671 applies to all figures in the contribution.

672 **Figure 5:** Zircon U-Pb results for the East George V Land paragneiss xenoliths 12GL02 and
673 04. (a,b) Wetherill diagrams. Error ellipses are quoted at 2σ level of uncertainty. (c,d)
674 Average ages calculated for the youngest concordant zircon population following the
675 $\text{YC}2\sigma(3+)$ estimator of Dickinson and Gehrels (2009). (e,f) Zircon U-Pb date distribution
676 represented as Kernel Density Estimates. Only analyses discordant at less than 10% are
677 displayed. All Kernel Density Estimates were plotted with the Density Plotter program of
678 Vermeesch (2013).

679 **Figure 6:** Zircon and monazite U-Th-Pb results for the George V Land paragneiss xenolith
680 12GL01. (a) Wetherill diagram showing zircon U-Pb data. Error ellipses are quoted at 2σ
681 level of uncertainty. (b) $^{206}\text{Pb}/^{238}\text{U}$ versus $^{208}\text{Pb}/^{232}\text{Th}$ diagram for the analyzed monazite
682 grains. Error ellipses are quoted at 2σ level of uncertainty.

683 **Figure 7:** U-Pb date distribution of zircon grain cores and rims from all samples, represented
684 as Kernel Density Estimates. Only analyses discordant at less than 10% are displayed.

685 **Figure 8:** Zircon U-Pb date distributions of the George V Land paragneiss xenoliths
686 compared to the main periods of geological activity (magmatism/metamorphism) in the Terre
687 Adélie craton (see text for references and discussion). Is also depicted an histogram
688 summarizing available intrusion ages for the Gawler craton (meta)igneous rocks. For
689 paragneisses zircon data, only analyses discordant at less than 10% are displayed. Data for the
690 Gawler craton are from the Geochron database of the Australian Geological Survey.

691 **Figure 9:** Detrital zircon U-Pb date distributions of the George V Land paragneiss xenoliths
692 compared to those of several Ediacaran to Lower Cambrian (meta)sediments from the
693 Delamerian segment of Australia, all represented as Kernel Density Estimates. Only analyses

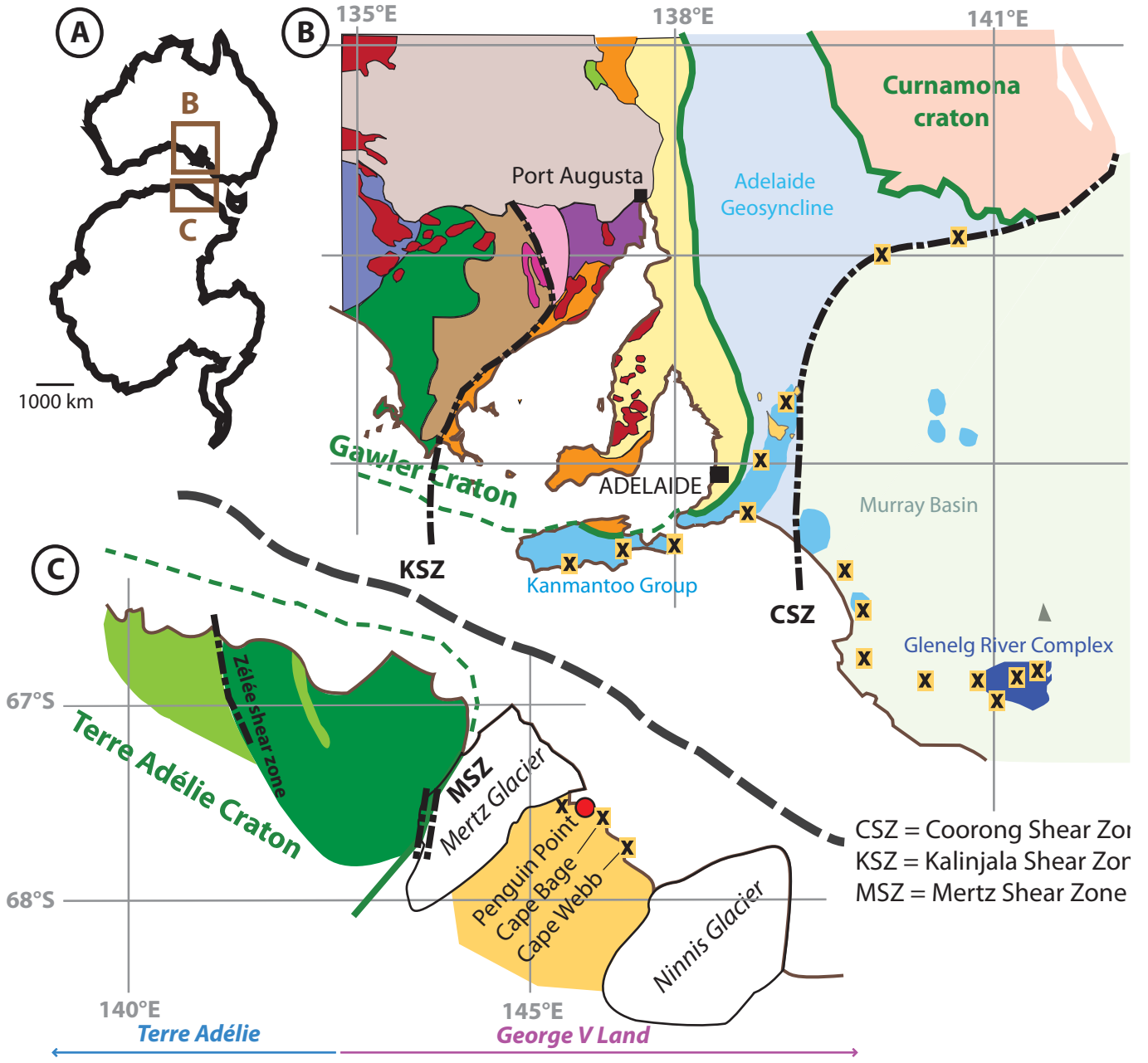
694 discordant at less than 10% are displayed. Data sources: Ireland et al. (1998) for Kanmantoo,
695 Normanville and Adalaidian sediments; Geochron database from the Australian Geological
696 Survey for the Nargoon group sediments (East Victoria).

697 **Supplementary material**

698 **Table 1:** Results of zircon and monazite U-Pb dating performed on gneiss xenoliths from

699 Eastern George V Land.

700



Pre-Kimban units west of the KSZ-MSZ (Mawson continent)	Pre-Kimban units east of the KSZ-MSZ	Post-Kimban units
<ul style="list-style-type: none"> Hutchinson Group (≥ 1850 Ma) Miltalie Gneiss (2000 Ma) Sleaford and Terre Adélie complexes (2560-2500 Ma) 	<ul style="list-style-type: none"> Wallaroo Group (1760 Ma) Myola Volcanics (1790-1740 Ma) Donington Suite (1850 Ma) Basement (3150 Ma) 	<ul style="list-style-type: none"> Hiltaba Suite (1590-1575 Ma) Gawler Range Volcanics (1600-1585 Ma) St Peter Suite (1620 Ma) Southern Curnamona Province (1715-1585 Ma)
<ul style="list-style-type: none"> Dumont d'Urville and Cape Hunter basins (≈ 1700 Ma) 		<ul style="list-style-type: none"> Paleozoic granites (≈ 500 Ma) Paleozoic deposits <ul style="list-style-type: none"> Murray Basin Nargoon Group Kanmantoo and Normanville Groups Adelaide Geosyncline

Figure 2

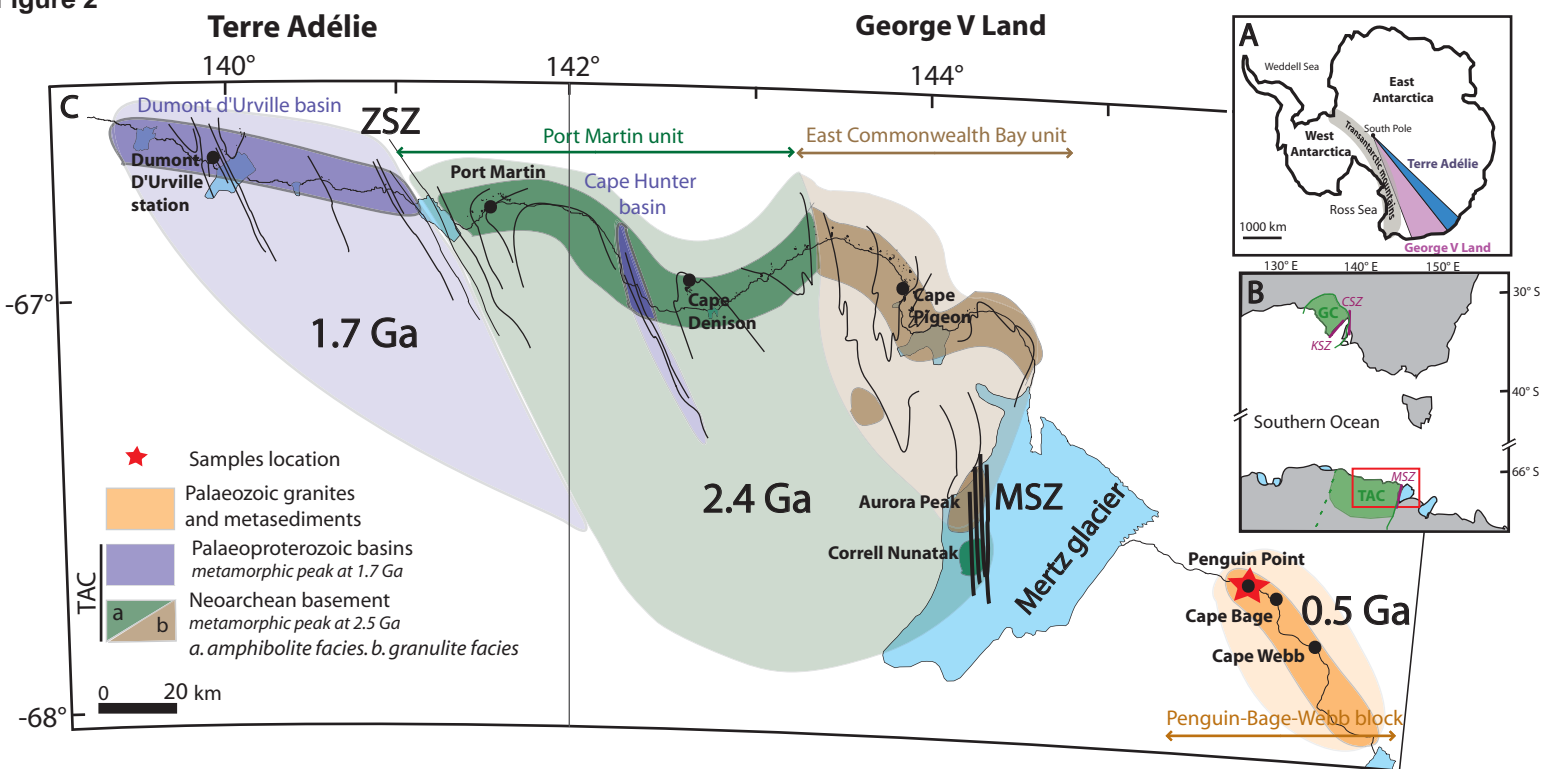


Figure 3
[Click here to download high resolution image](#)

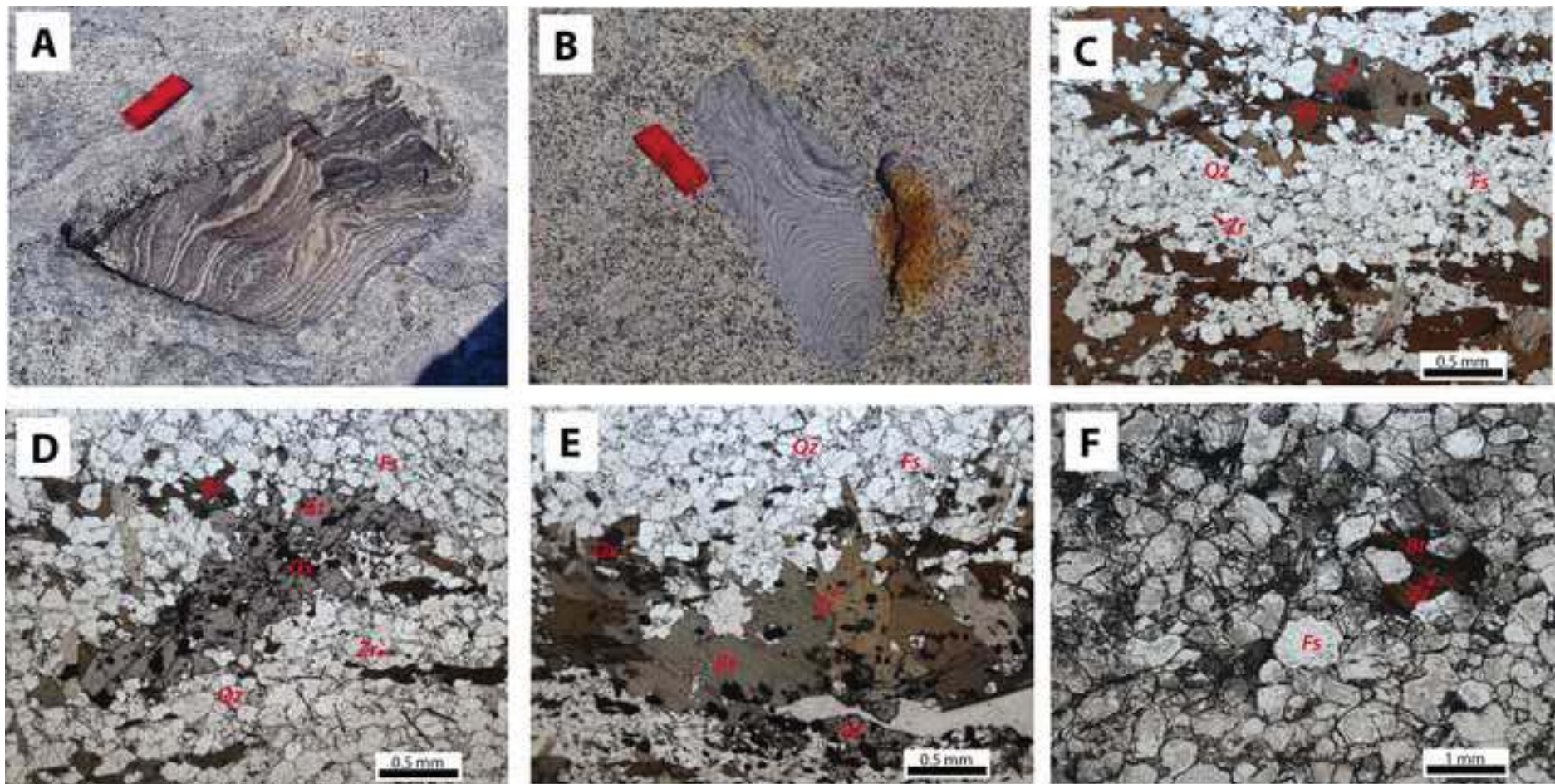


Figure 4
[Click here to download high resolution image](#)

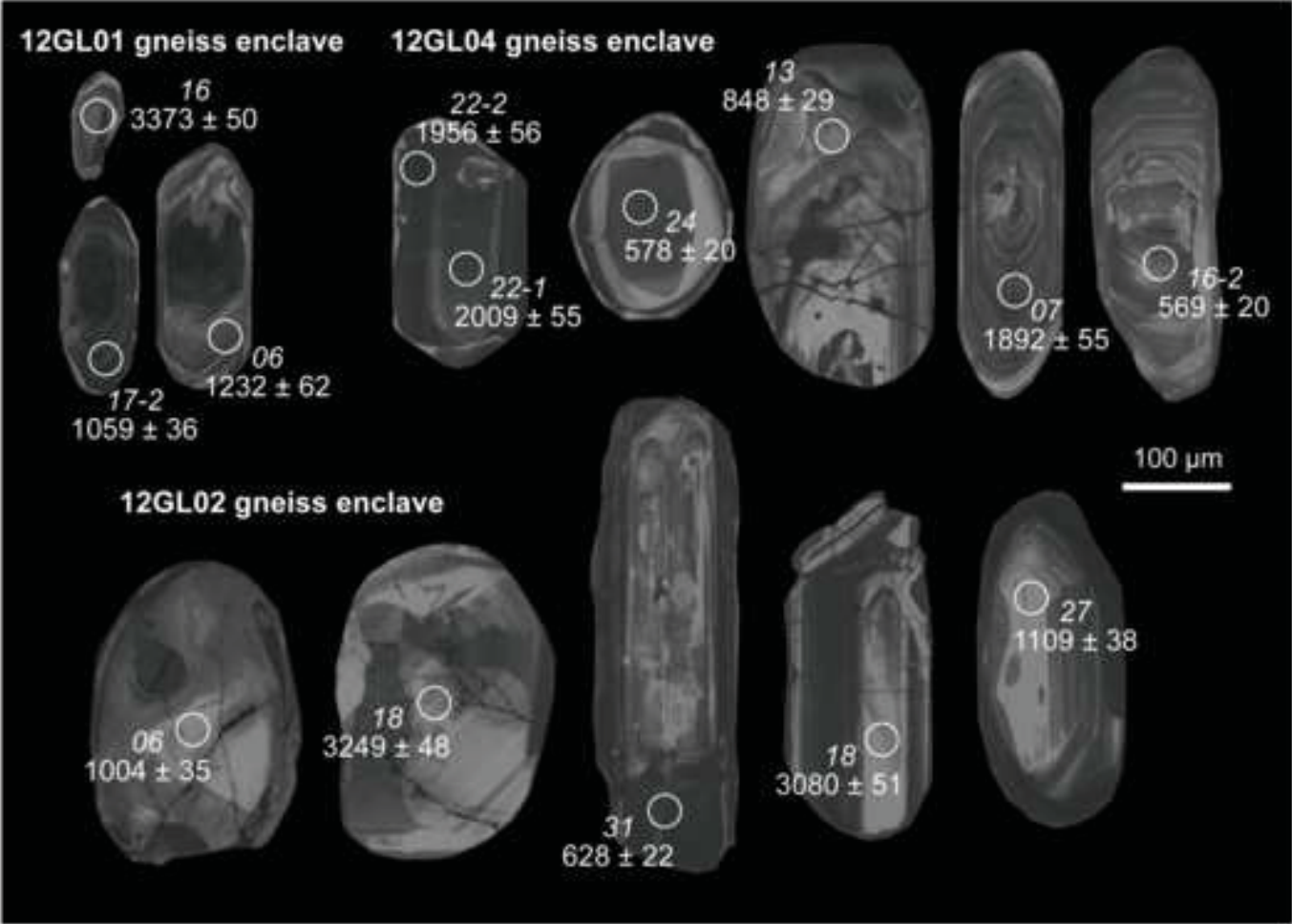


Figure 5

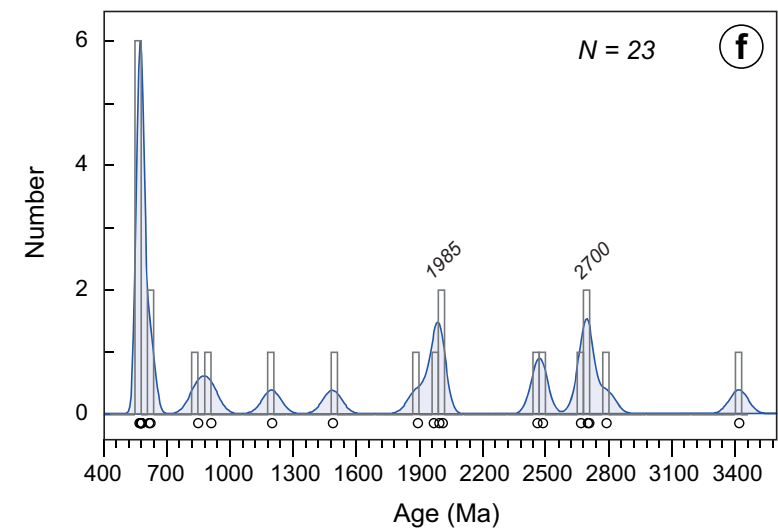
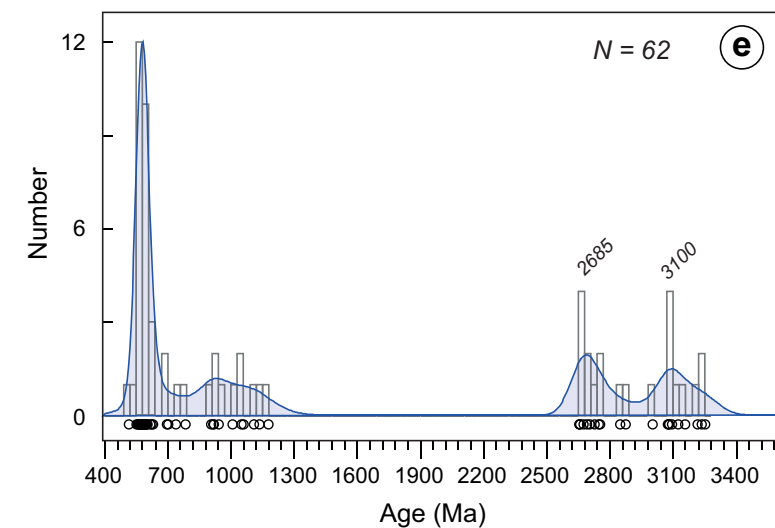
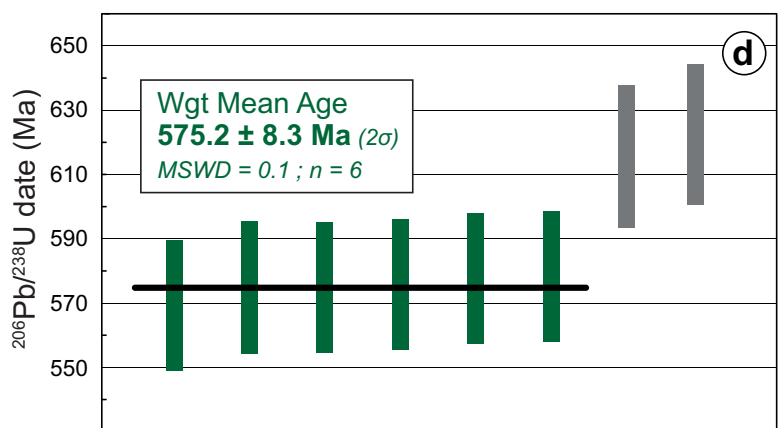
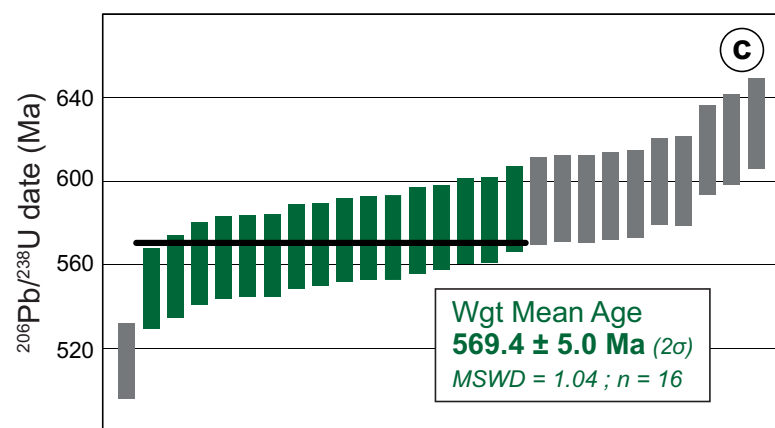
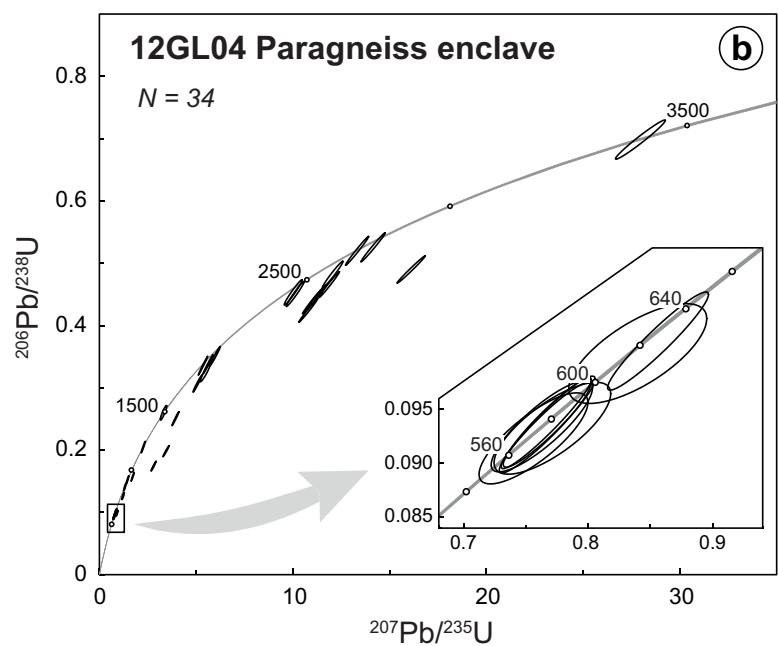
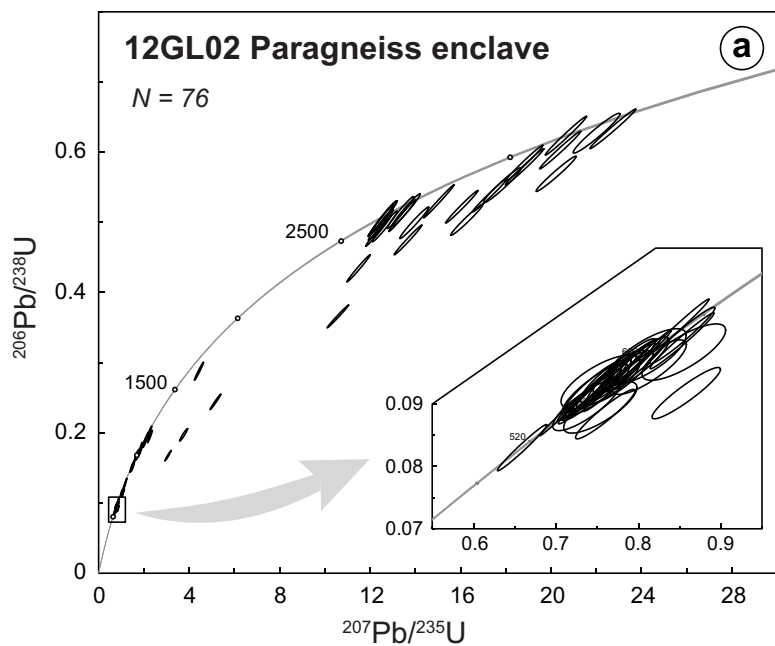


Figure 6

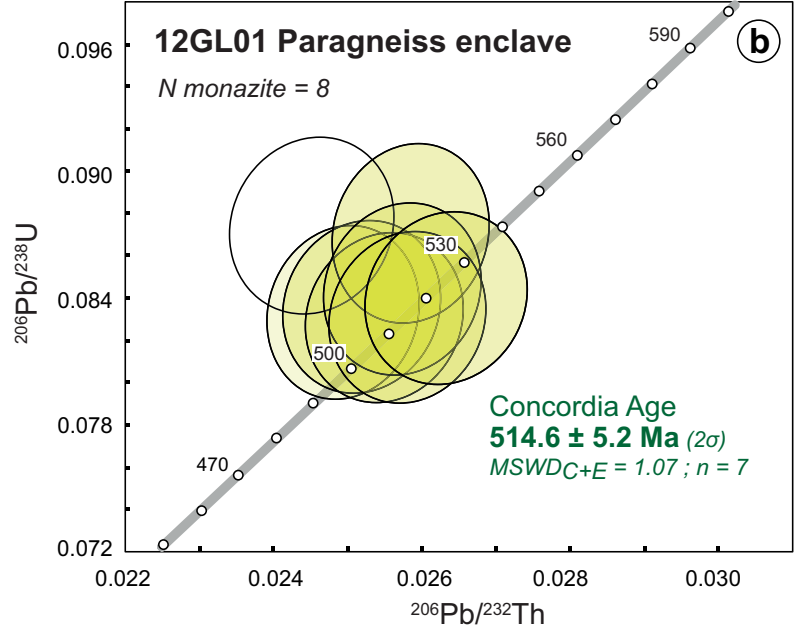
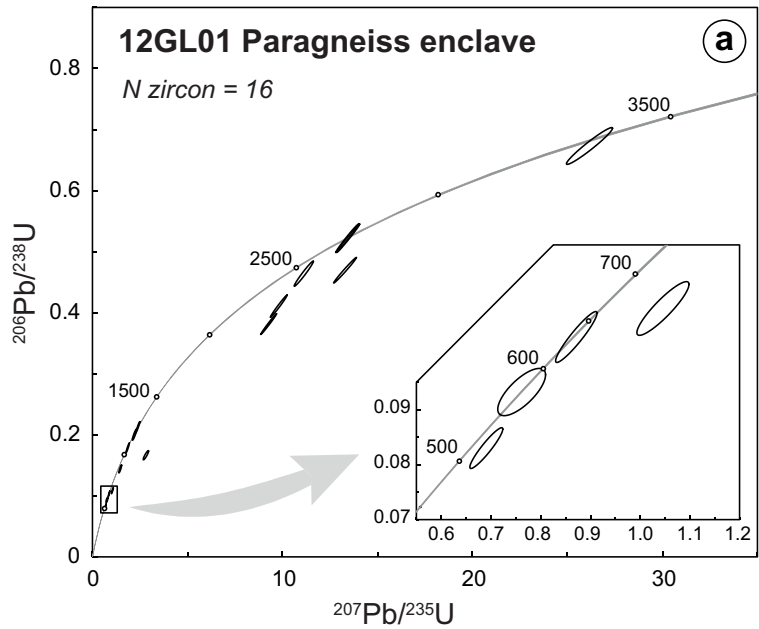


Figure 7

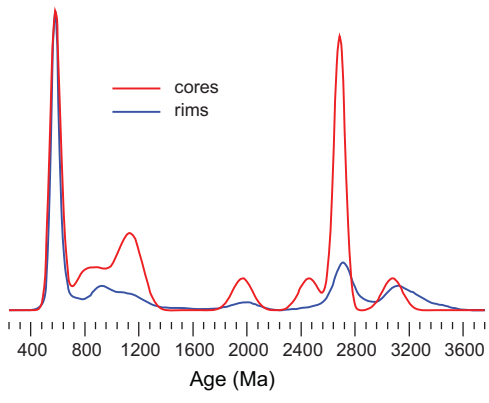


Figure 8

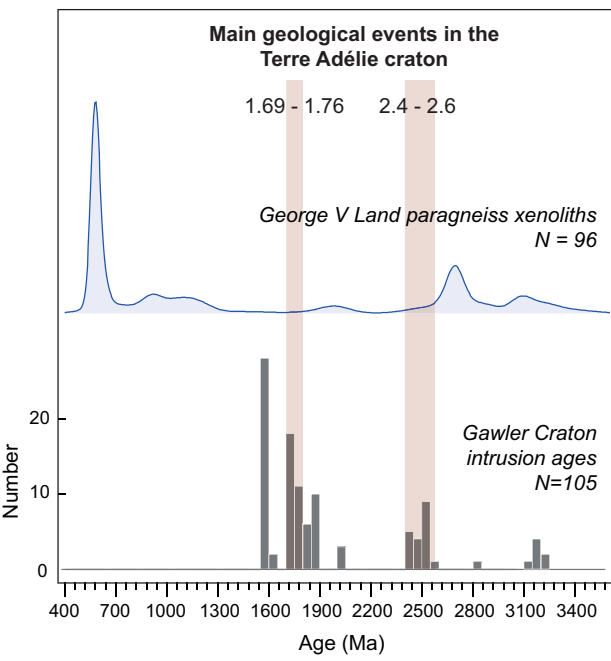
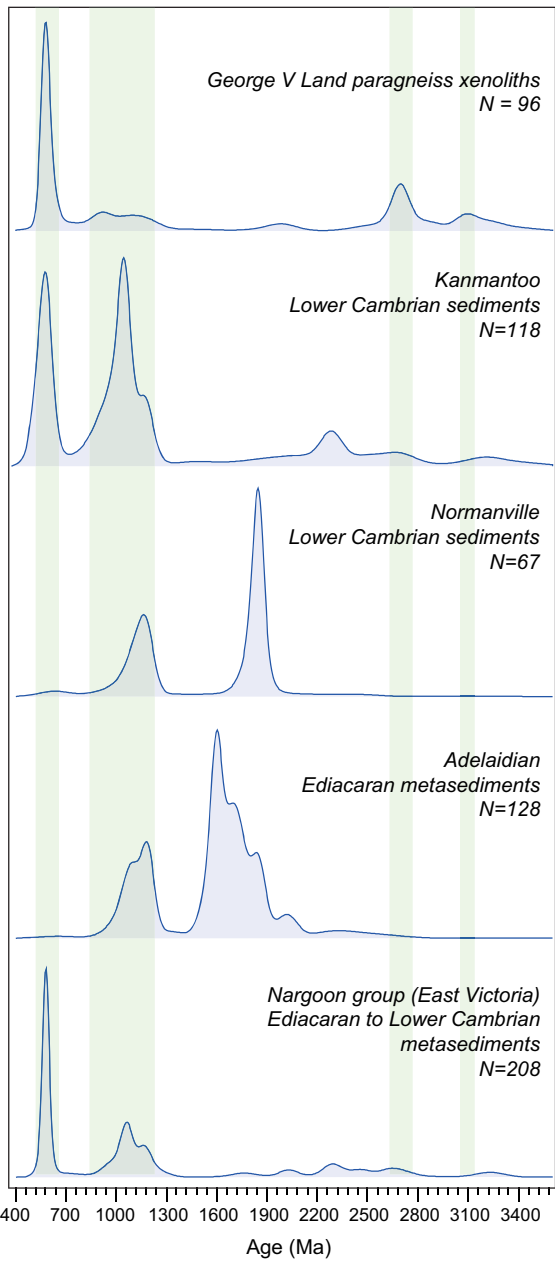


Figure 9



Background dataset for online publication only

[Click here to download Background dataset for online publication only: supplementary-data.xlsx](#)